Nanoscale

Accepted Manuscript

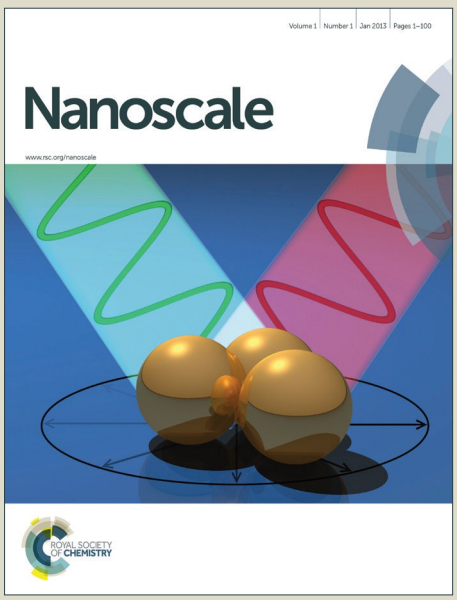

ROYAL SOCIETY OF CHEMISTRY

www.rsc.org/nanoscale

Journal Name

ARTICLE TYPE

Cite this: DOI: 10.1039/xxxxxxxxxx

Three dimensional inverse design of nanopatterns with block copolymers and homopolymers†

Dan Xu,[a] Hong Liu,*[a,b]‡, You-Liang Zhu,[c] and Zhong-Yuan Lu*[a]¶

Received Date
Accepted Date

DOI: 10.1039/xxxxxxxxxx

www.rsc.org/journalname

We propose a facile inverse design strategy to generate three-dimensional (3D) nanopatterns by using either block-copolymers or binary homopolymer blend via dissipative particle dynamics simulations. We find that the composition window of block copolymers to form specific 3D morphology can be expanded when the self-assembly of block copolymers is directed by templates. We also find that binary homopolymer blend can serve as better candidate in the inverse templating design, since they have similar performance on recovering the target pattern, meanwhile with much lower cost. This strategy is proved efficient on fabricating templates with desired topographical configuration, and the inverse design idea sheds lights on better control and design of materials with complex nanopatterns.

1 Introduction

Self-assembly of block copolymers (BCPs) on patterned template had been extensively investigated[1–22] for their multitudinous characteristics of morphologies. As representative structures assembled by BCPs, periodic lines, sharp 90° bends and three/four-way junctions have potential applications in nanomanufacturing functional devices[22]. Templates that direct the self-assembly of BCP films are mostly etched as columns in lines with long-range order. Regularly arranged cylindrical morphologies can be achieved on these confined templates. A lot of works, including computational studies, had focused on producing the layer of BCP thin film nanostructures directed by pre-designed templates[17–23]. Numerous works had also targeted to find optimized chemically patterned substrates which can direct the formation of ordered BCP structures[24–26]. In most previous computational approaches, researchers generally followed the so-called "forward" strategy, i.e., designing a set of humps with different geometries "standing" on the template and then finding the optimum morphology. These "forward" studies validated and even predicted new morphologies in experiments[15–17,23,26–29]. Nevertheless, the limitation of this strategy is that: It only works well for nanolithography when the target morphology contains simple or periodic features. Once the morphology is complex or nonperiodic (e.g., junction, bend, or even multideck three-dimensional structure), it becomes rather difficult to find the most suitable template using this "forward" design strategy, since a large parameter space has to be scanned.

Recently, Alexander-Katz and the co-workers proposed an algorithm that used a random optimization procedure combined with self-consistent field theory (SCFT) to inversely design nanopatterns that can direct BCP self-assemblies[30,31]. They applied this algorithm to determine the topographical configuration of template features for the BCP self-assembly into a predetermined target pattern[30,31]. In their study, the two-dimensional posts (simplified as small squares), which were attractive to the minority or majority block of the BCPs, initially had a random spatial distribution. Then a stochastic minimization process was conducted to optimize the positions of the posts based on the target pattern. The inverse design procedure involves finding optimized post distribution based on desired surface nanopatterns; therefore it successfully avoids scanning large parameter space, and in principle can determine possible topographical template for any target pattern. Other than its potential application on the nanolithography, this inverse design also sheds lights on the synthesis of tailored hierarchical and heterogeneous mesoscale materials[30]. Compared to most of the reported works following the "forward" strategy, i.e., designing different geometries on the template and then finding the optimum morphology in a trial and error fashion, the inverse design strategy is quite advanced for obtaining appropriate topographical shape of the template when the final pattern is clearly requested but the template is unknown. It is a new strategy of directed design of the nanopatterns by polymers.

[a] Institute of Theoretical Chemistry, State Key Laboratory of Supramolecular Structure and Materials, Jilin University, Changchun 130021, China
[b] Eduard-Zintl-Institut für Anorganische und Physikalische Chemie, Technische Universität, Darmstadt 64287, Deutschland
[c] State Key Laboratory of Polymer Physics and Chemistry, Changchun Institute of Applied Chemistry, Chinese Academy of Sciences, Changchun 130022, China
† Electronic Supplementary Information (ESI) available: [details of any supplementary information available should be included here]. See DOI: 10.1039/b000000x/
‡ hongliu@jlu.edu.cn.
¶ luzhy@jlu.edu.cn.

In this study, we propose to use dissipative particle dynamics (DPD) simulation method to inversely design templates for directed BCP self-assembly. With soft potential adopted in DPD, consequently polymer dynamics in melt is always Rouse-type and the simulations can be greatly accelerated. Moreover, in DPD simulation, free energy barriers can be naturally overcome due to inherent dynamics driven by thermal fluctuation in the system. Our inverse design strategy based on DPD can easily reproduce the result of Ψ-like nanopattern reported in ref. [30]. Since the relatively low computational cost of DPD, our inverse design strategy can reasonably expand to a three dimensional (3D) space with the nanoparticle (NPA) as the building block. Regularly and periodically arranged 3D pattern enables diverse applications of BCP such as solar cells and 3D printings[32,33]. More importantly, we introduce to use binary homopolymer blend (BHB) as the templating matrix, replacing BCP that is commonly used in conventional patterning. Our simulations show equal performance of BHB with BCP for obtaining the target morphology. If the template is properly constructed, this study demonstrates the possible application of homopolymers as the matrix of nanolithography by using inverse design strategy, since the homopolymers are technically easy to be synthesized and extremely cheaper as compared to BCPs.

2 Method and Model

DPD is a well-known mesoscopic simulation technique, which had been used to study various types of polymer systems. In DPD method, the time evolution of the interacting particles is governed by Newton's equations of motion[34] . Interparticle interactions are characterized by pairwise conservative F_{ij}^C, dissipative F_{ij}^D, and random forces F_{ij}^R acting on a particle i by a particle j. They are given by:

$$\begin{aligned} \mathbf{F}_{ij}^C &= \alpha_{ij}\omega^C\left(r_{ij}\right)\mathbf{e}_{ij}, \\ \mathbf{F}_{ij}^D &= -\gamma\omega^D\left(r_{ij}\right)\left(\mathbf{v}_{ij}\cdot\mathbf{e}_{ij}\right)\mathbf{e}_{ij}, \\ \mathbf{F}_{ij}^R &= \sigma\omega^R\left(r_{ij}\right)\xi_{ij}\Delta t^{-1/2}\mathbf{e}_{ij}. \end{aligned} \quad (1)$$

where $\mathbf{r}_{ij}=\mathbf{r}_i-\mathbf{r}_j$, $r_{ij}=|\mathbf{r}_{ij}|$, $\mathbf{e}_{ij}=\mathbf{r}_{ij}/r_{ij}$, and $\mathbf{v}_{ij}=\mathbf{v}_i-\mathbf{v}_j$. ξ_{ij} is a random number with zero mean and unit variance. $\omega^C\left(r_{ij}\right)=1-r_{ij}$ for $r_{ij}<1$ and $\omega^C\left(r_{ij}\right)=0$ for $r_{ij}\geq 1$ such that the conservative forces are soft and repulsive. The weight functions $\omega^D\left(r_{ij}\right)$ and $\omega^R\left(r_{ij}\right)$ of the dissipative and random forces couple together to form a thermostat. Español and Warren showed the correct relations between the two functions[35]:

$$\begin{aligned} \omega^D(r) &= \left[\omega^R(r)\right]^2, \\ \sigma^2 &= 2\gamma k_B T. \end{aligned} \quad (2)$$

We take a simple choice of $\omega^D(r)$ due to Groot and Warren[34]:

$$\omega^D(r)=\left[\omega^R(r)\right]^2=\begin{cases}(1-r)^2 & (r<1)\\ 0 & (r\geq 1)\end{cases}. \quad (3)$$

It should be noted that the choice of $\omega\left(r_{ij}\right)$ is not unique and is the simplest form adopted here because of its common usage in roughly all published works. α_{ij} is the repulsion strength, which takes the value of 25 for the particles of same kind in our simulations[34]. The parameter α_{ij} between differing species is often set as larger than 25, representing the degree of compatibility between them. In this study, the particle density $\rho=3$. The relationship between α_{ij} and Flory-Huggins parameter χ cites from[36]:

$$\alpha_{ij}=\alpha_{ii}+3.27\chi(\rho=3). \quad (4)$$

All the data reported in the following are in reduced units: the interaction cutoff distance, the bead mass and the temperature are set to be units, i.e. $r_c=m=k_BT=1$. The periodic boundary condition is applied in all three dimensions. The solid NPA is used as the building block of template. It is constructed by extracting all the beads belonging to a sphere (with predefined radius) from equilibrated DPD liquid configuration (of the same density $\rho=3$) and then setting them as a rigid body[37]. The advantage of this method is that the density and structure of solid NPA are completely the same as those of the DPD fluid. Therefore density fluctuation at the boundaries of solid NPAs and polymer bulk[38] can be reasonably eliminated. In this study, we choose the NPA radius $r_{NPA}=2.0$. The DPD simulation time step is set as $dt=0.02$ and for each system a period of at least 1×10^6 steps simulation is conducted for obtaining the equilibrium data. All simulations are performed using GALAMOST[39] package on Nvidia GTX780 GPU cards.

We choose a 3D periodic symmetrical structure as the desired pattern to describe our inverse design protocol. Suppose we need a pattern that is made by perpendicularly crossing three groups of stripes, with each group having four rectangularly arranged parallel and equidistant stripes of A-type species in a simulation box, as shown in Fig. 1a. This structure has eight 6-way junctions in the simulation box and looks like a Chinese character "water well" in cross-sectional view from each side of the simulation box, thus we call this target pattern as the "3D water well" pattern. The complementary region in the simulation box is filled with B-type species, incompatible to the A-type. Here we construct a cubic simulation box with size 40^3 and set the width of the A stripe as $L=8$, thus the volume fraction of A species is around $f_{A0}=0.35$ in the target pattern. The incompatible binary homopolymer blend A_5/B_5 (the chain length $N=5$) is used to form the target 3D well pattern, i.e., the A_5 homopolymer chains and B_5 homopolymer chains are respectively filled in their own regions with the bulk density. To better keep the 3D water well pattern, immobile hard frames are inserted in the interfaces of A and B species. For the modeling of the frames in DPD simulations, we can easily identify the number of the hard frames and their respective positions according to the shape of target pattern. Basically, the hard frames are constructed by orderly packing frozen DPD beads (designated as "F" type) to form a long right-angle wall. Firstly, a layer of regularly arranged and densely packed frozen F-type beads are utilized to form a surface of the frame, like the procedure in our previous work in which a flat substrate was constructed for the surface-initiated polymerization[40]. Then

it is copied into two surfaces. One of them is rotated for 90° and then translated appropriately, so that the two perpendicular surfaces can contact and form a compact right-angle wall. This wall model is further copied into several ones. Each wall is rotated appropriately and then moved to different positions as the frame to stabilize the local shape of the target pattern. In practice, between two frames we set that there are enough spaces so that the NPAs can diffuse through. During the simulations, the F-type frame beads are set immobile so that the frozen hard frames can keep the target 3D water well pattern unchanged. Please see Fig. 1a for the local architecture of frame. The DPD interaction parameter between the frame bead (F) and any other type of bead i is set as $\alpha_{iF} = 25$, indicating the neutral effect of the frame on the target pattern[40]. It should be noted that, we have observed that some block beads could pass through the frame during the simulation. However this penetrable frame model actually provides a better choice to modulate A and B domain interface, since the penetrable frame does not perturb the block bead density distribution at the interface as compared to impenetrable frame. Moreover, the frames are virtually introduced only for keeping the target pattern; they will be removed in the second step of inverse design. Therefore, we do not need to worry about the casual penetration of block beads through the frames in our simulations. Similarly, we find that a very small portion of beads can casually move into the NPAs. However, the global density of the bulk BHB or BCP of the inverse design does not decrease in a noticeable way. Thus this nonphysical phenomenon could not affect the self-assembly behavior of the matrix polymer chains.

The first step of inverse design is to determine the optimized distribution of NPAs (or topographical configuration of the template) according to the target pattern. In this step, the target pattern is kept basically stabilized by the hard frames while the NPAs can move in the simulation box. At the beginning of the simulations, after the construction of all the frames as stated above, a number of NPAs are distributed randomly in the simulation box but avoid the positions of frames (Fig. 1a). The filling of polymers to generate the target pattern is as follows. After the construction of all the frames as stated above, we start to fill the binary homopolymer blend A_5/B_5 to generate the target pattern. The simulation box is divided into several cubic parts of different sizes according to the shape of the target pattern. Since it is clear that in which cube the component A or B should be filled, the short A_5 and B_5 polymer chains are generated in their respective regions until the target bead number density is achieved. Each of the short chains is generated randomly in its predefined region. Firstly the position of the head monomer of the chain is determined randomly in the region. Each of the following 4 monomers of the same chain is generated one-by-one according to the position of its former monomer of the chain (with spatially random position but the distance to its former monomer being set as the initial bond length). Once the trial position of a given monomer is out of its predefined region, we will discard this trial and generate another one, until its position is suitable. The same procedure is employed to avoid the initial penetration of polymers in NPAs. Since DPD uses soft potential, we do not need to worry about the local overlap between monomers. A short equilibration is followed up to eliminate the influence of the initial configuration. By this procedure, we can eventually generate the frame-stabilized target pattern without any polymers staying in wrong regions or crossing the frozen hard frames or NPAs. To represent the nature of NPAs with polymer brush layer coatings[16,41,42], the NPAs are initially set to be attractive to A_5 homopolymer and repulsive to B_5 homopolymer (the interactions of A with NPA is $\alpha_{AP} = 15$ and of B with NPA is $\alpha_{BP} = 45$). Then in the simulations the NPAs will diffuse in the simulation box to "find" their optimal positions according to different degrees of affinity of polymer components to the NPA. Finally, the NPAs will stay in the stripe region formed by A-type species in equilibrium (Fig. 1b). In this step we successfully find suitable distribution of NPAs based on predefined nanopatterns. In the following we want to know if these NPAs can be used as template to guide the formation of target patterns using either BCPs or BHBs.

When the first step of determining optimized distribution of NPAs is completed, the target pattern and the hard frames are both removed from the simulation box. Only the template formed by NPAs remains in the simulation box for the second step of inverse design (Fig. 1c). We will verify whether the target pattern can be reproduced by using polymers directed by this template. Now the NPAs are set frozen as the hard and immobile template. We first consider to use block copolymers as the matrix to generate the target pattern, thus in the beginning of the simulations, A_mB_n type BCPs (with $m < n$, i.e., A the minority and B the majority) are randomly generated in the rest of simulation box with the bulk density. More importantly, we also use binary homopolymer blend of A_m/B_n as polymer matrix in the simulations to check the possibility of generating target pattern by using cheaper synthetic homopolymers. When the simulation of the second step of inverse design is switched on, the BCPs or BHBs can move with the constraint formed by NPA-template. After equilibrium, the pattern formed by polymers directed by the NPA template can be obtained. If the pattern can basically reproduce the shape of the predefined target pattern (Fig. 1d), this inverse design protocol can be taken as successful and efficient. Regarding to the practical operation of making the template by NPAs frozen in the second step, in experimental community there exist feasible techniques for the fabrication of directed crystal structure of NPAs, such as vertical deposition, electrophoretic deposition, spin coating, convective self-assembly, colloidal epitaxy, electrostatic induced self-assembly and so on[43–47]. A part of these techniques had been successfully employed in nanoscopic 3D structuring fabrication. For example, Singh et al.[48] had proposed a single step approach to generate tunable 3D binary colloidal assemblies from a drying droplet of binary colloidal suspension over large areas independent of substrate surface chemistry. We believe some of these techniques should be effective to achieve the desired 3D shape of template using available building blocks.

3 Results and discussion

The inverse design protocol based on DPD can successfully reproduce the Ψ-like 2D pattern reported in ref. [30]. In our simulations, the target structure is set as intrinsically 3D but its pattern only shows on the transversal surface along XY plane. The

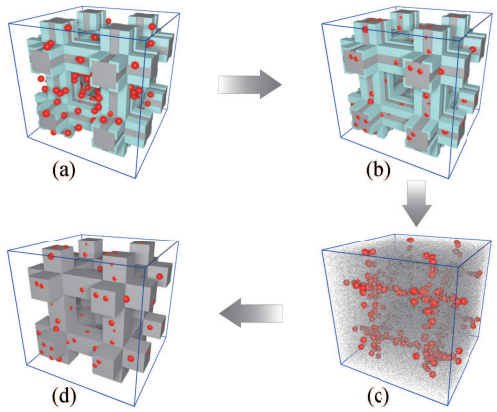

Fig. 1 Schematic flow chart of the inverse design strategy. (a) In the first step, the target pattern (gray) is kept sustainable by the hard frame (cyan) while the NPAs (red) can diffuse in the simulation box. (b) The NPAs will diffuse to "find" their optimal positions according to different degrees of affinity of polymer components to the NPA. After the equilibrium, only the template formed by NPAs remains in the box for the step of inverse design. (c) The NPAs are set frozen as the hard and immobile template. Then the BCPs or BHBs are used as polymer matrix and randomly generated in the rest of simulation box with bulk density, to see the possibility of reproducing target pattern. (d) After equilibrium of the simulation of inverse design, the pattern formed by the polymers directed by the NPA template can be obtained. If the pattern basically reproduces the predefined target pattern, this inverse design protocol can be taken as successful and efficient. The B species is not shown for clarity.

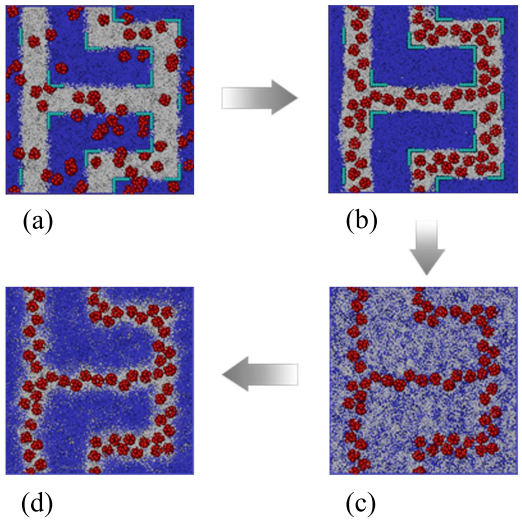

Fig. 2 Inverse template design to form the Ψ-like pattern. (a) In the first step, the goal is to determine the optimal positions of nanoposts which are used as the building blocks of template. The target pattern (gray) is kept sustainable by the frame (cyan) while the nanoposts (red) are put randomly in the box. (b) Nanoposts move into the target pattern region after the equilibrium. (c) We freeze the nanoposts as the hard template and remove all other components, and then randomly fill the rest space of box with BCPs with bulk density. (d) After equilibrium of the simulation of inverse design, the predefined target pattern can be formed by the BCPs directed by the nanopost template. All figures are obtained from the snapshots of our simulation.

nanoposts with the axes along the Z direction are chosen as the building blocks to form the template. Fig. 2 shows our inverse template design protocol, which is in essence the same as that shown in Fig. 1. The size of the box is set as $40\times40\times40$. The periodic boundary conditions are applied in all three dimensions. In the first step, the patterning structure made by the homopolymer blends (with two components A and B represented as gray and blue) is kept sustainable by the frames (cyan) while the nanoposts (red) are put randomly in the box. The feature width of A in the target pattern is set as 6, thus the volume fraction of A species is $f_A = 0.48$. In this step, the goal is to determine the optimal positions of nanoposts according to the target pattern. Only the translational motions of the nanoposts on the surface are considered. After equilibrium, in the second step, we freeze the NPOs as the hard template, remove other components and then fill in the rest of box with BCPs with bulk density. After DPD simulations, the patterning structure formed by the BCPs directed by the nanopost template can be obtained.

BCPs can naturally self-assemble to form various periodic morphologies depending on the composition ratio and incompatibility between components. In our simulations, we use BCPs with the volume fraction $f_A = 0.3$, which can easily form hexagonally packed cylindrical morphology in melt. The interaction parameter between BCP minority component A and nanoposts is set to be $\alpha_{AP} = 20$, while between BCP majority component B with nanoposts is set as $\alpha_{BP} = 30$, thus nanoposts favor the minority component slightly. The interaction parameter between the minority and the majority components of BCP is set as $\alpha_{AB} = 40$ to ensure microphase separation. As shown in Fig. 2c, in the second step of inverse design, the nanoposts are set frozen as the hard and immobile template and the free BCP chains are generated randomly in the simulation box. Fig. 2d shows that, after equilibrium of inverse design, the morphology induced by nanopost template can well reproduce the target Ψ-like pattern reported in ref. [30]. To demonstrate the similarity between equilibrium pattern induced by the template and the target pattern, we define an order parameter ϕ as

$$\phi = 1 - \frac{1}{M}\sum_{i=1}^{M}(f - f_0)^2 . \quad (5)$$

We first mesh the simulation box into $M = 40^3$ small cubic grids with the same side length of 1.0. f is defined as the volume fraction of minority beads at each grid of the obtained equilibrium pattern, while f_0 is that of the target pattern. Therefore the value of ϕ evaluates how much the obtained equilibrium pattern deviates from the target pattern. If $\phi = 1$, the obtained pattern completely reproduces the target pattern. When $\phi = 0$, the obtained pattern completely reverses the target pattern.

In the inverse design scheme, the reproducibility of target pattern induced by the template is primarily dependent on the polymer chain length and the number of nanoposts. For constant vol-

ume fraction $f_A = 0.3$ of BCPs (i.e. A_mB_n with $m/n = 3/7$), we systematically vary the chain length $N = m+n$ and the number of nanoposts (N_{NPO}) to find these influence on reproducing the target pattern. Fig. 3a shows that as the increase of N in the first stage when $N = 10 \sim 30$, ϕ increases sharply. The highest value of $\phi = 0.87$ appears when $N = 30$. Nevertheless, ϕ decreases as the further increase of N. For obtaining the best reproducibility of the target pattern, the feature width formed by BCPs should match the target pattern. When the chain length of BCP is less than $N = 30$, the domain sizes are too small to fit the structure of target pattern. The large domains formed by even longer BCP chains (e.g., $N > 30$) also do not fit the target pattern easily, as shown in the inset figures in Fig. 3a. Fig. 3b shows the dependence of order parameter ϕ on the number of nanoposts. The value of ϕ gradually increases from around 0.76 to a plateau value of 0.87 when $N_{NPO} = 50$. We find that if the number of nanoposts is too few, it is not effective to direct the self-assembly of BCPs. On the other hand, too many nanoposts are not economically advisable. Thus an optimal template with the appropriate numbers of nanoposts can be found in Fig. 3b (e.g., $N_{NPO} = 50$ in this system). We herein prove the reproducibility of this Ψ-like 2D pattern reported by Alexander-Katz[30], which had been validated in experiments (e.g., Fig. 1(c) and (d) of ref. [31]: SEM images of hydrogen silsesquioxane posts fabricated with electron beam lithography). This study can be considered as a comparison of the simulation work with experimental results. The general similar arrangement of nanoposts obtained in our simulations as that in experiment proves the feasibility of this simulation strategy for guiding future experiments.

Then we use this inverse design strategy to construct the "3D water well" pattern. Fig. 4a shows the dependence of ϕ on the BCP chain length N. As that in Fig. 3a, we fix the volume fraction $f_A = 0.3$ with variable chain length N. It is clear that with increasing BCP chain length, ϕ first increases to the peak value at around $N = 50$, then decreases to a smaller value. Only when the intrinsic feature width of the structure formed by BCPs, which is determined by the chain length, fits that of the target pattern, the latter can be reproduced satisfactorily. Therefore in the following, we set $A_{15}B_{35}$ with optimized chain length $N = 50$ as our BCP sample. Furthermore, this result may as well imply that BCP is not an ideal candidate to form target pattern, since it is not flexible enough to adjust its domain size which needs to fit well on the stripe width of the target pattern.

The number of NPAs, N_{NPA} affects the structural integrity of the template, which further affects the reproducibility of the predefined target pattern. In Fig. 4b, we plot the influence of N_{NPA} on ϕ. It shows that, as N_{NPA} increases from 70 to 170, the value of ϕ gradually increases to a plateau value at about 0.83. Then ϕ does not change apparently with N_{NPA}. As shown in Fig. 4b, when the amount of NPAs is not enough, it is difficult for the template to effectively direct the self-assembly of the BCPs to form target pattern. Thus a minimum number of NPAs is required to guarantee the reproduction of the target pattern effectively. However, using too many NPAs may bias the local morphology, meanwhile is not economic. As indicated in Fig. 4a and b, this inverse design scheme is also capable of finding the most suitable candidate

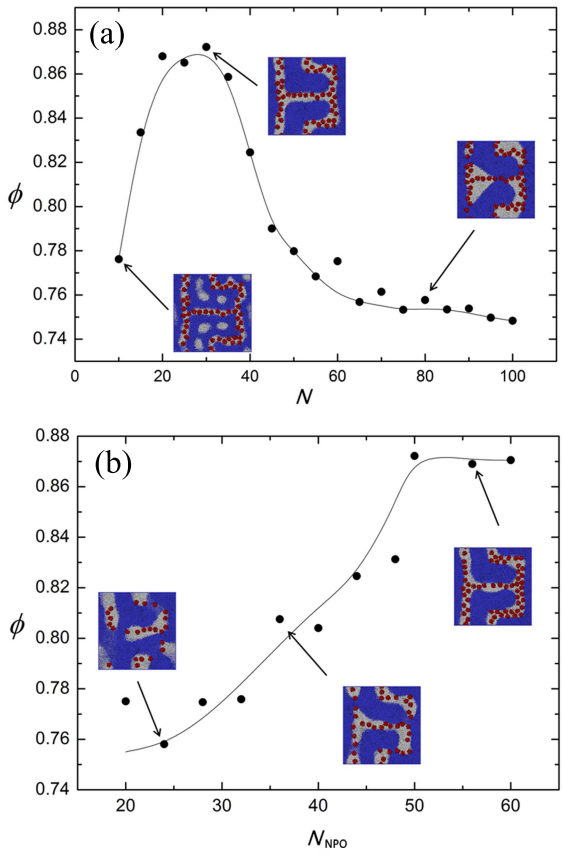

Fig. 3 (a) The dependence of order parameter ϕ on the BCP chain length N of the Ψ-like pattern. (b) The dependence of order parameter ϕ on the numbers of nanoposts (N_{NPO}) of the Ψ-like pattern. Both figures correspond to BCPs as the matrix.

polymer chain length and the minimum number of building block NPAs according to the target pattern.

According to the phase diagram of BCP microphase separation[33,49], the composition window corresponding to the cylindrical morphology is quite narrow. For example, when $\chi N > 30$, the range of volume fraction of the minority component should be controlled around $f_A = 0.2 \sim 0.3$ for obtaining the cylindrical morphology[50]. With the aid of directed BCP self-assembly by the template, there is a possibility to broaden this composition window since the template introduces additional interactions to BCPs. Here we use the structure factor to validate this speculation, which is often applied to characterize the specific microstructure of BCPs[51]. For further analyzing the regularity of the pattern, we introduce a new structure parameter τ based on the structure factor obtained from the patterns in our simulation. Firstly, the structure factor of the "3D water well" domain is calculated by[33,52]:

$$S(\vec{k}) = \rho_A(\vec{k})\rho_A(-\vec{k})/N_A,$$
$$\rho_A(\vec{k}) = \sum_{j=1}^{N_A} exp(i\vec{k}\cdot\vec{r_j^A}). \quad (6)$$

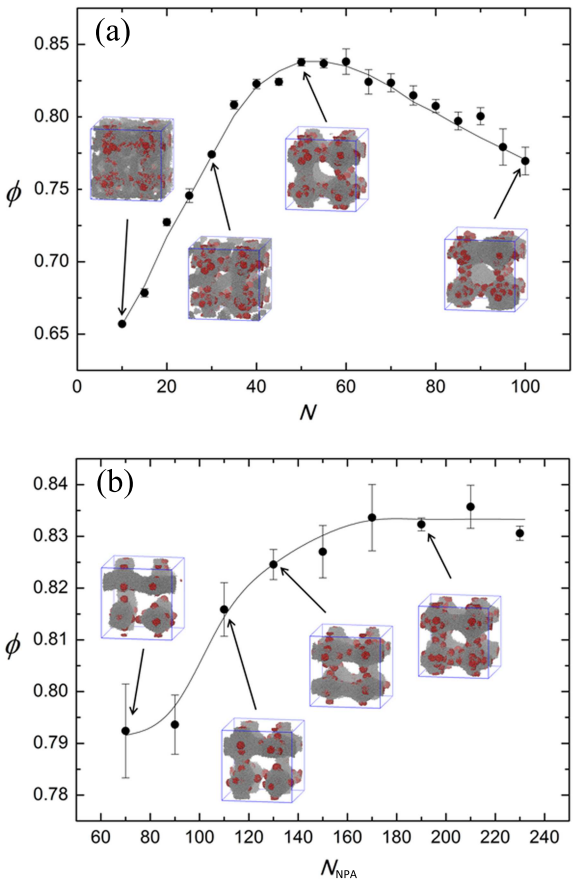

Fig. 4 (a) The dependence of order parameter ϕ on the BCP chain length N of the "3D water well" pattern. (b) The dependence of order parameter ϕ on the numbers of NPAs N_{NPA} of the "3D water well" pattern. Both figures correspond to BCPs as the matrix.

where N_A and $\rho_A(\vec{k})$ are the particle number and the density of "3D water well" domain in the reciprocal space, and L is the side length of simulation box. The integer wave number $\vec{k} = (L/2\pi)\vec{q}$, where $\vec{q}$ represents the wave vector. The differences between the structure factors of the obtained pattern in simulations and the predefined target pattern are calculated and their absolute values are summed up with the Bragg reflection ratio $q/q^* \leq 5$. Then the structure parameter τ is defined by

$$\tau = 1 \Big/ \sum_{q/q^*=1}^{5} \left| S_{\text{result}}(\vec{k}) - S_{\text{target}}(\vec{k}) \right| . \qquad (7)$$

Based on Eq. (7), we can evaluate the regularity of the pattern obtained in simulations as compared to the predefined target structures. The higher value of τ reasonably implies more regular pattern obtained in simulations and higher similarity as compared to the target pattern. We choose $N = 50$ since it has been proved to be the optimized chain length to fit the "3D water well" structure. By changing the value of f_A from 0.1 to 0.6, we simulate a series of systems of monodispersed BCPs and compare their morphologies directed by the template after equilibrium with the target pattern (for example, $f_A = 0.1$ denotes A_5B_{45} while $f_A = 0.6$ denotes $A_{30}B_{20}$). As shown in Fig. 5, the structure parameter τ first increases to a high value and then decreases slightly with the increase of f_A. We can basically find a range $f_A = 0.25 \sim 0.45$ in which τ has the highest value (i.e., above 2.5), and the predefined target pattern can be obtained. Such a composition window to observe cylindrical morphology is double the size as compared to pure BCP self-assembly in bulk. It can be attributed to the selectivity of the template to BCPs, which stabilizes the distributions of BCP minority as well as majority during their self-assembly. This effect weakens the dominant influence of the original driving force i.e., the incompatibility between the minority and majority, during BCP phase separation in bulk, which reasonably further enlarges the composition window of forming cylindrical morphology. The introduction of template may readily yield facilitated technology and cost saving in industrial production.

It should be noted that, regarding to this patterning strategy via NPAs as additives, the experimental work by Karim and co-workers need to be paid special attention. In this pioneering work[53], Karim and co-workers presented a simple and robust strategy for modulating the film-substrate interaction, which could bias the self-assembly energy landscape and thus enforce a desired microstructure. They used NPAs with tunable surface energy to generate a rough interface with controlled properties. By this technique they demonstrated a remarkable thickness-dependence of the induced orientation in the BCP lamellae. In a recent work by Karim and co-workers[54] involving both experiment and computer simulation, they studied the thermally-induced transition of lamellae orientation in BCP films on NPA-coated substrates, in which NPA-roughened substrate was used to modify substrate interaction and roughness, so that the BCP orientation could be controlled. In the above two studies by Karim et al., the NPAs were employed to modulate the physical and geometric property of the substrate, so that a directed desired microstructure of BCPs could be obtained. The idea is quite inspiring and relevant to our strategy, since the optimized NPAs arrangement on the substrate was possible to be designed based on the anticipated microstructure of BCPs.

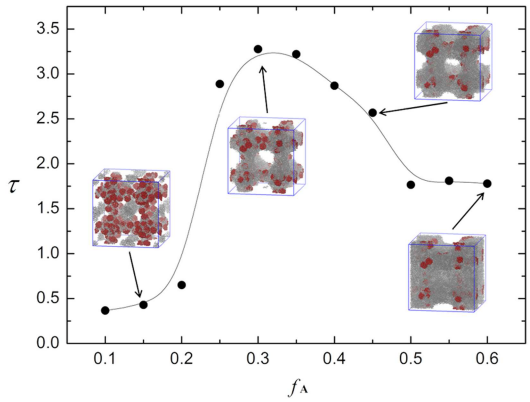

Fig. 5 The dependence of structure parameter τ on the volume fraction of the minority component in BCP, f_A at $N = 50$.

In general, incompatible binary homopolymer blends will phase separate to form macroscopic domains, thus are seldom taken as candidates to form ordered patterns, even though homopolymers are much cheaper and easy to be synthesized. In the following, we consider, based on designed template formed by NPAs, whether the BHBs are applicable as well to form predefined target patterns. A_{10}/B_{10} BHBs (with identical chain length $N = 10$) are taken as an example. In the simulations, the interactions of NPA with BHB are set as $\alpha_{AP} = 23$ and $\alpha_{BP} = 30$ to represent a slight preference of NPA to A-type species. The interaction between NPA and A_{10} of BHB is slightly larger than that between NPA and minority component in BCPs $\alpha_{AP} = 20$. This is because in practice based on the microphase separation of BCPs, a stronger attraction of A to NPA is requested for maintaining the regular structure. While with macroscopic phase separation of BHB, it is rational to set NPAs more neutral to the polymer so that there are less external perturbations. The interaction parameter α_{AB} in BHB as well as the volume fraction of A_{10} homopolymer (f_A) are important factors affecting the equilibrium pattern. Surprisingly, we find similar performance on reproducing target pattern by using BHBs as that by using BCPs in a suitable range of α_{AB} and f_A.

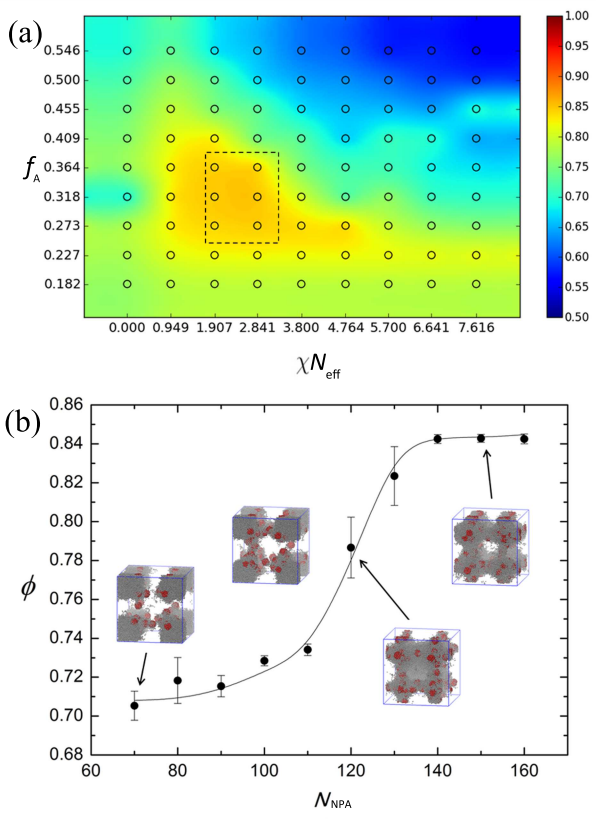

Fig. 6 (a) The dependence of order parameter ϕ on both volume fraction of A species, f_A, and incompatibility between A and B, χN_{eff}. (b) The dependence of order parameter ϕ on the number of NPAs N_{NPA}. The figures correspond to BHBs as the matrix.

DPD interaction parameter α can be reasonably translated to the commonly used Flory-Huggins χN_{eff} value corresponding to the Gaussian chain with infinite length[33]. Fig. 6a shows the "phase diagram" of the dependence of ϕ on both f_A and χN_{eff}. It is clear that it needs simultaneously appropriate ratio of A/B in BHB and incompatibility between A and B species to reproduce the predefined target pattern (see the region in orange color enclosed by the dashed rectangle with relatively higher ϕ in Fig. 6a). Since the original volume fraction of A species in the target pattern is $f_{A0} = 0.35$ (see Model and Method section), the values of f_A corresponding to the best reproduction should be around this value. Filling more A species or less A species is disadvantageous to the reproduction of target pattern. Moreover, within this range of f_A, too weak or too strong incompatibility between A and B species biases appropriate driving force of phase separation, which further reduces the reproducibility of the target pattern. The optimum parameter space is basically considered as $\chi N_{eff} = 1.91 \sim 2.84$ and $f_A = 0.27 \sim 0.36$ in this study. The theoretical order-disorder-transition point for homopolymer blends is $\chi N = 2.0$[55]. The optimum parameter space of $\chi N_{eff} = 1.91 \sim 2.84$ in our simulations implies that the ideal candidate as the BHB matrix to form predefined target pattern based on designed template should be the binary homopolymers with very weak incompatibility. It can be ascribed to that the template composed by the NPAs intrinsically has selectivity to one component of BHB, which helps the phase separation between A and B homopolymers and results in successfully recovering of target pattern. This result suggests a new possibility to choose suitable polymer systems for use in nanolithography.

We have also studied the dependence of ϕ on N_{NPA} for the reproduction of predesigned target pattern using BHBs. As shown in Fig. 6b, similar trend between ϕ and N_{NPA} as that using BCPs (Fig. 4b) can be observed, implying similar performance of reproducing target pattern using BHBs and BCPs as the matrix. This conclusion is also supported by the snapshots in Fig. 7. We can also find in Fig. 6b that 140 NPAs are enough to reproduce target pattern using BHBs, as compared to 170 NPAs using BCPs (Fig. 4b). In other words, with relatively incomplete template the BHBs can still recover the target pattern. Therefore, with lower cost and higher tolerance on template defect, BHBs are considered as better candidate compared to BCPs in the inverse templating design. This part of study emphasizes the possibility of an advanced alternative scheme that using BHBs instead of BCPs as the matrix in the formation of target pattern.

It should be noted that, although a direct comparison between our results with experiments that used homopolymer blends in 3D patterning is difficult, it has been a long time since the experimentalists employed BHB in the surface patterning to obtain 2D ordered structures. For example, the binary poly(2-vinylpyridine) (PVP) and polystyrene (PS) blend was frequently used on this issue. Steiner and co-workers[56] had shown that the domains of a phase-separating PVP and PS mixture in a thin film could be guided into arbitrary structures by a surface with a prepatterned variation of surface energies. Such a pattern could be imposed on a surface by using printing methods for depositing microstructured molecular films. Steiner et al.'s technique of using BHB for surface patterning is quite similar to ours, expect it was still based on a 2D templating. Moreover, Cui et al.[57] used pat-

terned sbustrate with alternating silicon dioxide and octadecyltrichlorosilane self-assembly monolayer (SAM) to induce phase separation of PS and PVP binary polyemr blend film. Raczkowska et al.[58] used PVP and brominated PS blends to spin-cast onto a gold substrate which had been microcontact-printed with stripes of hexadecanethiol SAM subpattern periodicity. These experimental studies support the feasibility of using BHB as the candidate in templating design. Regarding to the BHB in 3D structuring as proposed in our paper, we have not found any experimental work in previous literatures. Nevertheless, Léopoldès and Damman[59] had used the ethanol and polydimethylsiloxane liquid-liquid bilayer to obtain the 3D topology structuring through selective inversion of this bilayer. In their work the blend for the bilayer was ethanol and polydimethylsiloxane homopolymer instead of BHB, but this work implies the potential application of BHB for future 3D structure design, exactly as proposed in our paper. Since BHBs were proved to have similar performance as BCPs in templating design in our simulations, we believe they will be potentially widely applied as the candidate of templating design in experiments in the future.

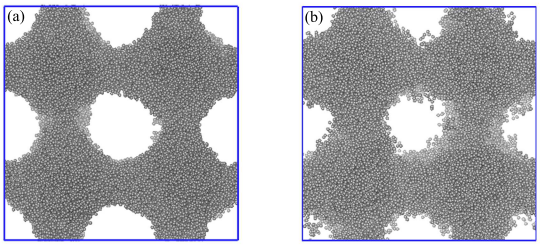

Fig. 7 With the "3D water well" structure as the target pattern, the final snapshots of the resulting patterns by the inverse design strategy from the cross-section view with (a) block copolymers (BCPs) and (b) binary homopolymer blends (BHBs) as the matrices. The matrix in the system of (a) is $A_{15}B_{35}$ type BCPs. The DPD interaction parameter between BCP minority component A and NPAs is set to be $\alpha_{AP} = 20$, while between BCP majority component B with NPAs is set as $\alpha_{BP} = 30$. The interaction parameter between the minority and the majority components of BCP is set as $\alpha_{AB} = 40$. The number of NPAs is $N_{NPA} = 180$. In the system of (b) the matrix is A_{10}/B_{10} BHBs. The DPD interactions of NPAs with BHB are set as $\alpha_{AP} = 23$ and $\alpha_{BP} = 30$. The interaction parameter between A and B is set as $\alpha_{AB} = 27$. The number of NPAs is $N_{NPA} = 150$. Similar performances on reproducing target pattern are found by using both BCPs and BHBs as the matrices.

4 Conclusions

In this study, we exhibit the inverse design strategy with both BCPs and BHBs as the matrix by DPD simulations. Two consecutive steps, i.e., the templating step and the inverse templating step, are included in the scheme. The successful reproduction of the Ψ-like nanopattern[30] proves the feasibility of this inverse design strategy using particle-based simulation techniques. A specific three-dimensional target pattern can be successfully reproduced by both BCPs and BHBs in the inverse templating process. By analyzing the structures of resulting pattern, we find by introducing the template in BCP self-assembly, the composition window for cylindrical morphology can be reasonably broadened, which may readily yield facilitated technology and cost saving in industrial production. We also find that BHBs with suitable incompatibility can serve as better candidate on recovering the predefined target pattern than BCPs, because they are much cheaper and can tolerate template defects while exhibit similar performance on recovering the target pattern. Particle-based dynamics simulation has natural advantage on finding suitable topographical configuration of template than direct template design, because it can easily construct the virtual movements of the building blocks of the template determined by the target pattern. This study sheds lights on better control and design of material with complex nanopatterns using nanolithography technique.

5 Acknowledgment

This work is subsidized by the National Basic Research Program of China (973 Program, 2012CB821500), and supported by the National Science Foundation of China (21474042, 21534004, 51273007). We also thank the supports from Jilin Province Science and Technology Development Plan (20140519004JH, 20140101096JC). H. L. gratefully acknowledges the support from the Alexander von Humboldt Foundation.

References

1 M. Luo, T. H. Epps,III, *Macromolecules*, 2013, **46**, 7567–7579.
2 K. Koo, H. Ahn, S.-W. Kim, D. Y. Ryu, T. P. Russell, *Soft Matter*, 2013, **9**, 9059–9071.
3 J. G. Son, A. F. Hannon, K. W. Gotrik, A. Alexander-Katz, C. A. Ross, *Adv. Mater.*, 2011, **23**, 634–639.
4 R. A. Mickiewicz, J. K. W. Yang, A. F. Hannon, Y.-S. Jung, A. Alexander-Katz, K. K. Berggren, C. A. Ross, *Macromolecules*, 2010, **43**, 8290–8295.
5 M. P. Stoykovich, K. Ch. Daoulas, M. Müller, H. Kang, J. J. de Pablo, P. F. Nealey, *Macromolecules*, 2010, **43**, 2334–2342.
6 S. Ji, C.-C. Liu, G. Liu, P. F. Nealey, *ACS Nano*, 2010, **4**, 599–609.
7 S.-M. Park, G. S. W. Craig, Y.-H. La, H. H. Solak, P. F. Nealey, *Macromolecules*, 2007, **40**, 5084–5094.
8 R. Ruiz, H. Kang, F. A. Detcheverry, E. Dobisz, D. S. Kercher, T. R. Albrecht, J. J. de Pablo, P. F. Nealey, *Science*, 2008, **321**, 936–939.
9 K. Galatsis, K. L. Wang, M. Ozkan, C. S. Ozkan, Y. Huang, J. P. Chang, H. G. Monbouquette, Y. Chen, P. Nealey, Y. Botros, *Adv. Mater.*, 2010, **22**, 769–778.
10 J. Y. Cheng, C. A. Ross, E. L. Thomas, H. I. Smith, G. J. Vancso, *Adv. Mater.*, 2003, **15**, 1599–1602.
11 R. A. Segalman, H. Yokoyama, E. J. Kramer, *Adv. Mater.*, 2001, **13**, 1152–1155.
12 Y. Dong, C. Dong, F. Wan, J. Yang, C. Zhang, *Sci. China Chem.*, 2015, **58**, 1515–1523.
13 L. Niu, J. Yan, X. Yang, C. Burger, L. Rong, B. Hsiao, D. Liang, *Sci. China Chem.*, 2014, **57**, 1738–1745.
14 L.-T. Yan, N. Popp, S.-K. Ghosh, A. Böker, *ACS Nano*, 2010, **4**, 913–920.
15 A. Tavakkoli K. G., A. F. Hannon, K. W. Gotrik, A. Alexander-

Katz, C. A. Ross, K. K. Berggren, *Adv. Mater.*, 2012, **24**, 4249–4254.
16 A. Tavakkoli K. G., K. W. Gotrik, A. F. Hannon, A. Alexander-Katz, C. A. Ross, K. K. Berggren, *Science*, 2012, **336**, 1294–1298.
17 J.-B. Chang, J. G. Son, A. F. Hannon, A. Alexander-Katz, C. A. Ross, K. K. Berggren, *ACS Nano*, 2012, **6**, 2071–2077.
18 J. K. W. Yang, Y. S. Jung, J.-B. Chang, R. A. Mickiewicz, A. Alexander-Katz, C. A. Ross, K. K. Berggren, *Nat. Nanotechnol.*, 2010, **5**, 256–260.
19 L. Zhang, L. Wang, J. Lin, *ACS Macro Lett.*, 2014, **3**, 712–716.
20 X. He, Z. Zou, D. Kan, H. Liang, *J. Chem. Phys.*, 2015, **142**, 101912.
21 J.-B. Chang, H. K. Choi, A. F. Hannon, A. Alexander-Katz, C. A. Ross, K. K. Berggren, *Nat. Commun.*, 2014, **5**, 3305.
22 M. P. Stoykovich, H. Kang, K. Ch. Daoulas, G. Liu, C.-C. Liu, J. J. de Pablo, M. Müller, P. F. Nealey, *ACS Nano*, 2007, **1**, 168–175.
23 C. T. Black, O. Bezencenet, *IEEE T. Nanotechnol.*, 2004, **3**, 412–415.
24 G. S.Khaira, J. Qin, G. P. Garner, S. Xiong, L. Wan, R. Ruiz, H. M. Jaeger, P. F. Nealey, J. J. de Pablo, *ACS Macro Lett.*, 2014, **3**, 747–752.
25 H. Yi, X.-Y. Bao, J. Zhang, C. Bencher, L.-W. Chang, X. Chen, R. Tiberio, J. Conway, H. Dai, Y. Chen, S. Mitra, H.-S. P. Wong, *Adv. Mater.*, 2012, **24**, 3107–3114.
26 J. Y. Cheng, C. T. Rettner, D. P. Sanders, H.-C. Kim, W. D. Hinsberg, *Adv. Mater.*, 2008, **20**, 3155–3158.
27 X. Xiao, Y. Huang, J. Feng, H. Liu, Y. Hu, *Marcomol. Theor. Simul.*, 2011, **20**, 124–132.
28 Q.-Y. Tang, Y.-Q. Ma, *Soft Matter*, 2010, **6**, 4460–4465.
29 P. Chen, H. Liang, R. Xia, J. Qian, X. Feng, *Macromolecules*, 2013, **46**, 922–926.
30 A. F. Hannon, K. W. Gotrik, C. A. Ross, A. Alexander-Katz, *ACS Macro Lett.*, 2013, **2**, 251–255.
31 A. F. Hannon, Y. Ding, W. Bai, C. A. Ross, A. Alexander-Katz, *Nano Lett.*, 2014, **14**, 318–325.
32 V. Ho, B. W. Boudouris, B. L. McCulloch, C. G. Shuttle, M. Burkhardt, M. L. Chabinyc, R. A. Segalman, *J. Am. Chem. Soc.*, 2011, **133**, 9270–9273.
33 Y. Li, H.-J. Qian, Z.-Y. Lu, A.-C. Shi, *Polymer*, 2013, **54**, 6253–6260.
34 R. D.Groot, P. B. Warren, *J. Chem. Phys.*, 1997, **107**, 4423–4435.
35 P. Espanõl, P. Warren, *Europhys. Lett.*, 1995, **30**, 191–196.
36 R. D. Groot, T. J. Madden, *J. Chem. Phys.*, 1998, **108**, 8713–8724.
37 M. P. Allen, D. J. Tildesley, *Computer Simulation of Liquids*; Clarendon: Oxford, U.K., 1987.
38 H.-J. Qian, L.-J. Chen, Z.-Y. Lu, Z.-S. Li, *Phys. Rev. Lett.*, 2007, **99**, 068301.
39 Y.-L. Zhu, H. Liu, Z.-W. Li, H.-J. Qian, G. Milano, Z.-Y. Lu, *J. Comput. Chem.*, 2013, **34**, 2197–2211.
40 H. Liu, M. Li, Z.-Y. Lu, Z.-G. Zhang, C.-C. Sun, *Macromolecules*, 2009, **42**, 2863–2872.
41 M. R. Bockstaller, Y. Lapetnikov, S. Margel, E. L. Thomas, *J. Am. Chem. Soc.*, 2003, **125**, 5276–5277.
42 C. Park, J. Yoon, E. L. Thomas, *Polymer*, 2003, **44**, 6725–6760.
43 S. H. Im, M. H. Kim, O O. Park, *Chem. Mater.*, 2003, **15**, 1797–1802.
44 N. V. Dziomkina, M. A. Hempenius, G. J. Vancso, *Adv. Mater.*, 2005, **17**, 237–240.
45 A. Mihi, M. Ocaña, H. Míguez, *Adv. Mater.*, 2006, **18**, 2244–2249.
46 A. V. Blaaderen, R. Ruel, P. Wiltzius, *Nature*, 1997, **385**, 321–324.
47 Z. Cheng, W. B. Russel, P. M. Chaikin, *Nature*, 1999, **401**, 893–895.
48 G. Singh, S. Pillai, A. Arpanaei, P. Kingshott, *Nanotechnology*, 2011, **22**, 225601.
49 M. W. Matsen, F. S. Bates, *J. Chem. Phys.*, 1997, **106**, 2436–2448.
50 M. W. Matsen, M. Schick, *Phys. Rev. Lett.* , 1994, **72**, 2660–2663.
51 A. J. Ryan, S.-M. Mai, J. P. A. Fairclough, I. W. Hamley, C. Booth, *Phys. Chem. Chem. Phys.*, 2001, **3**, 2961–2971.
52 J. Chai, F. Huo, Z. Zheng, L. R. Giam, W. Shim, C. A. Mirkin, *Proc. Natl. Acad. Sci. USA*, 2010, **107**, 20202–20206.
53 K. G. Yager, B. C. Berry, K. Page, D. Patton, A. Karim, E. J. Amis, *Soft Matter*, 2009, **5**, 622–628.
54 K. G. Yager, C. Forrey, G. Singh, S. K. Satija, K. A. Page, D. L. Patton, J. F. Douglas, R. L. Jones, A. Karim, *Soft Matter*, 2015, **11**, 5154–5167.
55 M. Rubinstein, R. H. Colby, *Polymer Physics*; Oxford, U.K., 2003.
56 M. Böltau, S. Walheim, J. Mlynek, G. Krausch, U. Steiner, *Nature*, 1998, **391**, 877–879.
57 L. Cui, Z. Zhang, X. Li, Y. Han, *Polymer Bulletin*, 2005, **55**, 131–140.
58 J. Raczkowska, A. Bernasik, A. Budkowski, J. Rysz, B. Gao, M. Lieberman, *Macromolecules*, 2007, **40**, 2120–2125.
59 J. Léopoldès, P. Damman, *Nat. Mater.*, 2006, **5**, 957–961.